PHYSICAL REVIEW E **80**, 061902 (2009)

Aggregation of chemotactic organisms in a differential flow

Javier Muñoz-García*
School of Mathematical Sciences and Complex and Adaptive Systems Laboratory, Systems Biology Ireland, and Grupo Interdisciplinar de Sistemas Complejos (GISC), University College Dublin, Belfield, Dublin 4, Ireland

Zoltán Neufeld
School of Mathematical Sciences and Complex and Adaptive Systems Laboratory, University College Dublin, Belfield, Dublin 4, Ireland
(Received 30 December 2008; revised manuscript received 9 October 2009; published 4 December 2009)

We study the effect of advection on the aggregation and pattern formation in chemotactic systems described by Keller-Segel-type models. The evolution of small perturbations is studied analytically in the linear regime complemented by numerical simulations. We show that a uniform differential flow can significantly alter the spatial structure and dynamics of the chemotactic system. The flow leads to the formation of anisotropic aggregates that move following the direction of the flow, even when the chemotactic organisms are not directly advected by the flow. Sufficiently strong advection can stop the aggregation and coarsening process that is then restricted to the direction perpendicular to the flow.

DOI: 10.1103/PhysRevE.80.061902 PACS number(s): 87.18.Hf, 47.63.−b, 82.39.Rt, 87.18.Ed

I. INTRODUCTION

Directed motion of microorganisms and cells in response to chemical signals —*chemotaxis*—plays an important role in a wide range of biological processes including migration of white blood cells, cancer invasion [1], embryonic development or in locating nutrients by bacteria, algae, etc. [2,3]. In many cases the chemotactic cells not only detect, but also produce chemical signals that may attract other members of the population. This type of communication based on chemoattractant odors or pheromones can control group behavior, aggregation, swarming, and collective decisions (quorum sensing) in bacterial colonies [4], slime mold [5], or insect populations. Often the medium into which the chemical signal is released is not stationary but is a moving fluid (e.g., air or water) while the chemotactic cells or organisms are not transported by the flow as their motility is restricted to crawling on a solid surface. For example, microorganisms may attach to surfaces developing biofilms [6] found in natural environments or bioreactors and on a wide variety of surfaces, including living tissues, pipings, and industrial or medical devices. The interface between a surface and an aqueous medium such as water or blood provides an ideal environment for the development of microorganisms. The growth and structure of biofilm communities is a complex process regulated by the properties of the cell surface, diverse characteristics of the medium, type of substratum, and hydrodynamics of the aqueous medium. The influence of hydrodynamics on biofilm structures has been studied recently [7–9] and was shown that the current velocity affects the structure and dynamics of natural biofilms resulting in different colony shapes [9]. In Ref. [10] is described the use of "slow" laminar flows (from 100 μm s^{-1}) to pattern cell culture substrate in capillary systems. Another interesting property that may influence the structure of biofilms is the cell-to-cell signaling or quorum sensing. For example, in Ref. [11] the importance of intercellular molecule signaling on biofilm differentiation is studied.

The response of attached cells to a shear flow and the effects of cell-to-cell signaling on the aggregation have been also studied for a particular slime mold: the *Dictyostelium discoideum*. Using a laminar flow Décavé and co-workers established the critical shear stress for *D. discoideum* cells on glass [12] and studied the mechanisms responsible for the induced enhanced motility [13]. On the other hand the aggregation of *D. discoideum* by means of secreting cyclic adenosine monophosphate (cAMP) has been modeled using stochastic and discrete approaches; the continuum descriptions of cell aggregation have been mostly employed and later derived from mechanistic and microscopic descriptions [14]. The mathematical properties of these equations are relevant for a broad range of models that have been developed to understand the aggregation process in a variety of organisms, pigmentation patterning, neural crest migration, inflammatory response, tumor growth, etc.

In this work we will study the simultaneous effect of differential advection and cell-to-cell signaling on the aggregation and pattern formation of chemotactic biological populations using a model of partial differential equations to describe the evolution of the cell density and the chemical signal concentration. The resulting system is similar to the nonlinear chemical reactions studied by Rovinsky and Menzinger involving activator and inhibitor kinetics where a differential flow can induce a pattern forming instability [15,16].

II. MODEL

A well known classical continuum model of chemotaxis at the population level is the Keller-Segel (KS) model [5] that describes the evolution of the density of chemotactic cells, $u(\mathbf{x},t)$, and the chemoattractant concentration, $v(\mathbf{x},t)$, at point $\mathbf{x}$ and time t. When the chemical field v is advected by a uniform flow $\mathbf{V}$ and the density field evolves on a fixed substrate, we have

*javiermunozgarcia@gmail.com; http://gisc.uc3m.es/~javier

$$\partial_t u = \nabla \cdot [D_u \nabla u - \chi(u) \nabla v], \tag{1}$$

$$\partial_t v = D_v \nabla^2 v + fu - sv - \mathbf{V} \cdot \nabla v, \tag{2}$$

where D_u and D_v are constant diffusivities. The chemoattractant is assumed to be produced proportionally to the local cell density (with a constant of proportionality f) while it is degraded with a frequency s. Although in Ref. [13] it was shown that a shear flow increases the cell motility in *D. discoideum*, since we will consider slower flow velocities than in Ref. [13] (which were on the order of the detachment velocity), in Eq. (1) we assume that representative values of D_u are closer to those measured in the absence of flow such as in Ref. [17]. Assuming no-flux or periodic boundary conditions the total mass of the biological component is conserved and can be characterized by the average density. In the original KS model [5,18] $\mathbf{V}=0$ and the chemotactic flux is proportional to the particle density, i.e., $\chi(u)=\chi_0 u$. Extensions of this model with more general forms for $\chi(u)$ have also been studied such as the chemotaxis model with the prevention of overcrowding introduced in Ref. [19] where $\chi(u)=\chi_0 u(1-u/u_{max})$ with u_{max} as the maximum allowed cell density. An important feature of the KS model (observed in biological systems such as slime mold populations) is that it demonstrates an aggregation instability when the total mass of cells is larger then a certain threshold. Properties of the solutions of the KS system and its variants have been studied extensively (for recent reviews, see Refs. [14,20,21]). Interesting analogies between KS-type chemotaxis models and nonlinear mean-field Fokker-Planck equations and generalized thermodynamics have been pointed out in [22].

In order to simplify the analysis of Eqs. (1) and (2) we introduce nondimensional variables by rescaling $x' \mapsto (s/D_v)^{1/2} x$, $t' \mapsto st$, $u' \mapsto u_0^{-1} u$, and $v' \mapsto s(fu_0)^{-1} v$, with u_0 as the initial mean cell density, resulting in the following system:

$$\partial_t u = \nabla \cdot [D \nabla u - \chi(u) \nabla v], \tag{3}$$

$$\partial_t v = \nabla^2 v + u - v - \mathbf{V} \cdot \nabla v, \tag{4}$$

where we have defined $D \equiv D_u/D_v$, $\chi(u)' \equiv f/(sD_v)\chi(u)$, $\mathbf{V}' \equiv (sD_v)^{-1/2}\mathbf{V}$, and omitted primes. In order to estimate the typical spatial and temporal scales in this problem we can use parameter values given in Ref. [18] for the chemoattractant cAMP: $D_v \sim 10^{-6}$ cm^2 s^{-1} and $s \sim 1$ s. Thus, the typical units for the rescaled length, time, and velocity are on the order of 0.1 μm, 1 s, and 10 μm s^{-1}, respectively.

It is important to note that for *D. discoideum* the critical shear stress for detachment on glass is on the order of $\sigma_{1/2} \approx 2.6$ Pa [12]. For low Reynolds number when the inertial effects can be neglected the wall shear stress on the adhering cells is proportional to the uniform velocity following $\sigma = 6\eta V/d$, where η is the dynamic viscosity of the fluid and d is the distance between the top of the chamber and the substrate. Using $d=0.25$ mm as in Ref. [13] and water at room temperature ($\eta=10^{-3}$ Pa s), we obtain an estimate for the detachment velocity: $V_{1/2} \approx 10^5$ μm s^{-1}. Thus, as we will see below, the flow velocities considered here are smaller than the velocity needed to detach the cells from the substrate and we can assume that the organisms are not advected by the flow, although they are still able to move by crawling on the solid surface as represented by the chemotactic and diffusive terms.

III. LINEAR ANALYSIS

In order to gain insight into the system we consider the stability of the spatially uniform solution. Assuming uniform initial conditions for u and v with $v(t=0) \equiv v_0$ all spatial derivatives vanish in Eqs. (3) and (4) and we have the solutions $u(t)=1$ and $v(t)=1+(v_0-1)e^{-t}$. Thus, independent of the initial conditions the concentration tends to 1 for large times. To investigate pattern forming instability in this system, we consider the evolution of spatially nonuniform periodic perturbations added to the uniform steady state of the form $u(\mathbf{x},t)=1+\hat{u}\exp[i\mathbf{q}\cdot\mathbf{x}+\omega(\mathbf{q})t]$ and $v(\mathbf{x},t)=1+\hat{v}\exp[i\mathbf{q}\cdot\mathbf{x}+\omega(\mathbf{q})t]$ and study whether the perturbation is amplified or damped out in the course of time. Here, $\mathbf{q}$ is the wave vector of the perturbation, $\omega(\mathbf{q})$ is the corresponding dispersion relation, and $\hat{u}$ and $\hat{v}$ are the amplitudes of the perturbation at $t=0$. Substituting these expressions into Eqs. (3) and (4) and neglecting quadratic terms in $\hat{u},\hat{v}$, we obtain a linear system of equations where nontrivial solutions only exist if the determinant of the coefficient matrix is equal to zero. In contrast to previous chemotactic models where advection is not considered (see, for example, [23] for a linear stability study of an inertial model generalizing the KS model), the resulting quadratic equation for the dispersion relation has complex coefficients and reads

$$\omega^2 + \omega(a+ib) + (c+id) = 0. \tag{5}$$

The coefficients a, b, c, and d are functions of parameters and wave-vector components yielding

$$a = (D+1)q^2 + 1, \tag{6}$$

$$b = \mathbf{V} \cdot \mathbf{q}, \tag{7}$$

$$c = Dq^4 + [D - \chi(1)]q^2, \tag{8}$$

$$d = Dq^2 \mathbf{V} \cdot \mathbf{q}. \tag{9}$$

The real and imaginary parts corresponding to the two complex solutions are (see, for example, p. 95 of [24])

$$\mathrm{Re}(\omega^{\pm}) = -\frac{a}{2} \pm \frac{1}{2\sqrt{2}}\{[(a^2-b^2-4c)^2 + (2ab-4d)^2]^{1/2} + a^2 - b^2 - 4c\}^{1/2}, \tag{10}$$

$$\mathrm{Im}(\omega^{\pm}) = -\frac{b}{2} \pm \frac{\mathrm{sgn}(2ab-4d)}{2\sqrt{2}}\{[(a^2-b^2-4c)^2 + (2ab-4d)^2]^{1/2} - a^2 + b^2 + 4c\}^{1/2}. \tag{11}$$

The real part of ω gives the growth or decay rate of the perturbation amplitude. In particular, the mode corresponding to the maximum of $\mathrm{Re}(\omega)$, which we denote by $\mathbf{q}^l$, determines the characteristic wavelength of the pattern in the

linear regime, while the imaginary part describes its propaation in space. The velocity $\mathbf{V}^l$ at which the instability travels across the substrate, corresponding to the *phase velocity* of the mode $\mathbf{q}^l$, satisfies the relationship [25]

$$\mathbf{V}^l \cdot \mathbf{q}^l = -\mathrm{Im}[\omega(\mathbf{q}^l)]. \tag{12}$$

The negative branch of the dispersion relation is unconditionally stable, i.e., $\mathrm{Re}(\omega^-) < 0$, but the positive branch may produce nontrivial dynamics and pattern formation for a certain range of wave numbers. Some insight into the behavior of the system can be obtained by investigating the limiting cases of small and large wavelengths. For large values of q we can expand Eq. (10) to obtain $\mathrm{Re}(\omega^+) = -Dq^2$; therefore, the amplitude of perturbations decays exponentially for these modes. In the case of large-wavelength perturbations the expansion to the lowest orders in q yields

$$\mathrm{Re}(\omega^+) = [\chi(1) - D]q^2 - \chi(1)q^2\{[1 - D + \chi(1)]q^2 + (\mathbf{V} \cdot \mathbf{q})^2\} + \mathcal{O}(q^6). \tag{13}$$

Thus, when $\chi(1) - D > 0$ the positive branch has a band of unstable modes for small wave vectors. In the case of the standard KS model, $\chi(1) = \chi_0$, the above condition is equivalent to the aggregation threshold: $D/\chi_0 < 1$ [5,18]. In Eq. (13) we observe that the advection velocity appears at the order q^4. This means that, when the above condition for instability is satisfied, there is always a band of unstable modes with long wavelengths around $q = 0$, but the range of unstable modes and their growth rate decrease with the advection velocity. This stabilizing effect of the flow is in contrast with the behavior of reaction-diffusion systems studied by Rovinsky and Menzinger [15,16] where the differential flow induces an instability at a finite wavelength. For the imaginary part of ω, we have the following expansion of Eq. (11) for small wave vectors:

$$\mathrm{Im}(\omega^+) = -\chi(1)q^2(\mathbf{V} \cdot \mathbf{q}) + \mathcal{O}(q^5). \tag{14}$$

Therefore, although the particle density is not directly advected by the flow, using Eq. (12) we see that the chemotaxis induces a phase velocity $\mathbf{V}^l$ that is inversely proportional to the square of the wavelength and, consequently, it is small relative to the advection velocity.

IV. PATTERN FORMATION IN ONE DIMENSION

Figure 1(a) shows the effect of the advection velocity on the real part of the dispersion relation given by Eq. (10) for a one-dimensional (1D) system. When V increases the wave number of the dominant mode corresponding to the maximum of $\mathrm{Re}(\omega^+)$, q^l, decreases [Fig. 1(b)]. In fact, from the expansion of Eq. (10) for small q given by Eq. (13) we have $q^l = [\nu/(2\mathcal{K})]^{1/2}$ with $\nu = \chi(1) - D$ and $\mathcal{K} = \chi(1)[(1-D) + \chi(1) + V^2]$. Thus, for large V, the dominant wavelength in the linear regime, $\lambda^l = 2\pi/q^l$, is proportional to the advection velocity. The phase velocity of the spatial pattern [Eq. (12)] is also shown in Fig. 1(b) as a function of the advection velocity for the exact dispersion relation [Eq. (11)]. We notice that the phase velocity has a maximum for a certain value of V. Thus, surprisingly, when the advection velocity is increased beyond this value, the phase velocity of the pattern decreases as V is increased. This nonmonotonic dependence can also be shown using the expansion of $\mathrm{Im}(\omega^+)$ for small wavenumber modes [Eq. (14)] from where a compact analytical expression for the phase velocity is obtained [see Fig. 1(b)],

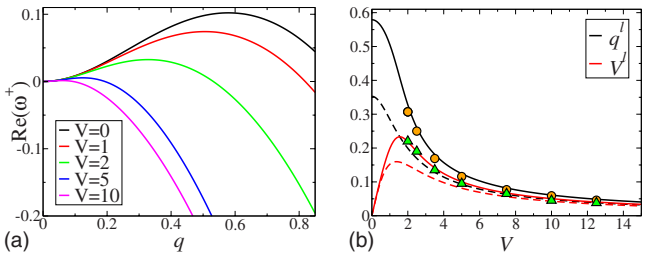

FIG. 1. (Color online) (a) Real part of the dispersion relation $\mathrm{Re}(\omega^+)$ given by Eq. (10) as a function of q for a 1D system with $\chi(u) = \chi_0 u(1 - u/u_{max})$, for $D = 1$, $\chi_0 = 2.5$, $u_{max} = 4$, and different values of the advection velocity (from top to bottom) $V = 0$, 1, 2, 5, and 10. (b) Linear dominant mode q^l (black lines) and phase velocity V^l [red (gray) lines] as functions of the advection velocity. The solid lines represent the exact solution obtained from Eqs. (10) and (11). The dashed lines represent the approximate solution for small wavelengths. The velocity of the pattern and the dominant mode measured from the numerical simulations are represented by triangles and circles, respectively.

$$V^l = \chi(1)V(q^l)^2 = \frac{[\chi(1) - D]V}{2[(1 - D) + \chi(1) + V^2]}. \tag{15}$$

Although this expression is only valid for small values of q^l, it is qualitatively similar to the exact solution and already shows that V^l increases linearly for small values of V and when the advection velocity exceeds a certain threshold, $V_t = \sqrt{(1-D) + \chi(1)}$, larger values of V induce a slower pattern movement.

It is interesting to discuss how the linear wavelength and the phase velocity are modified when D is decreased since in typical experiments $D_u/D_v \ll 1$. For strong advection we can use the expansion of Eq. (10) for small q to obtain the minimal value of the linear wavelength. Since in the aggregation regime, $0 < D < \chi(1)$, the linear wavelength is an increasing function of D, for $D \to 0$ we obtain $\lambda^l_{min} = 2^{3/2}\pi\sqrt{1 + \chi(1) + V^2}$, from where we see that the linear wavelength becomes larger when the chemosensitivity is increased. On the other hand, V_t is a decreasing function of D. Thus, in the limit $D \to 0$ the maximum phase velocity is reached when the advection is $V_t = \sqrt{1 + \chi(1)}$. Therefore, as we could expect, the efficiency of the particles following the chemical field depends on the chemosensitivity. For larger values of $\chi(1)$ the cells can more accurately follow the chemical field up to larger values of the advection velocity.

For the numerical simulations we use the chemotactic response function: $\chi(u) = \chi_0 u(1 - u/u_{max})$ that avoids the singularities associated with other models. Interestingly, we have also found that, in the case of the standard linear response, $\chi(u) = \chi_0 u$, advection can suppress the singularity and produce qualitatively similar behavior to the previous function when V is sufficiently large. We consider periodic boundary

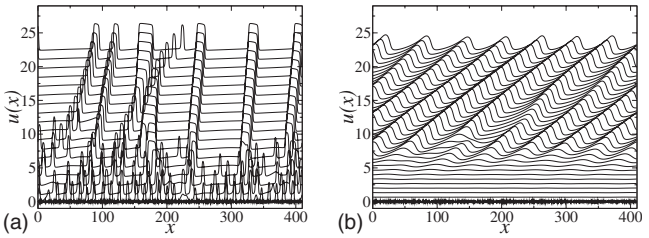

FIG. 2. (a) Particle density profiles at equally spaced times (profiles are offset vertically) between $t=0$ (bottom) and $t=3500$ (top) for (a) $V=1$ and (b) $V=5$.

conditions with initial fields in the uniform steady state with a small amplitude random perturbation. The parameters in Eqs. (3) and (4) were set to $D=1$, $\chi_0=2.5$, and $u_{max}=4$ for the one- and two-dimensional (2D) simulations.

Representative one-dimensional numerical simulations of the particle density profiles $u(x,t)$ are shown in Fig. 2 for two different values of the advection velocity. In the case of $V=1$ [Fig. 2(a)] we observe a slow coarsening process which tends to reduce the number of structures as observed in the system without advection [19]. However, for $V=5$ [Fig. 2(b)] after a short transient a periodic pattern with a constant wavelength develops. As shown in Fig. 2, in the presence of advection the $x\to -x$ symmetry of the profiles is broken [see also Fig. 3(a)] and the pattern propagates in the positive direction (i.e., in the direction of the advection velocity). In the absence of coarsening (i.e., for values of $V\gtrsim 2$) the pattern moves uniformly with a well-defined velocity as shown in Fig. 2(b). The velocity of the pattern was measured for different values of V and is plotted in Fig. 1(b). The measured velocity agrees well with the analytical results obtained from the linear stability analysis. Independent of the initial chemical concentration, after a transient time the behavior of the chemoattractant v is very similar to the density profiles, as shown in Fig. 3(a) where the profiles of u and v are plotted together for different values of V. For large advection velocities the particles cannot "follow" the chemical gradients, the two profiles are more different and the aggregates are more spread out. Figure 3(b) shows the temporal evolution of the wavelength $\lambda(t)$ (measured as two times the average distance between consecutive minima and maxima) for different values of V. Aggregation starts earlier for larger values of V, and

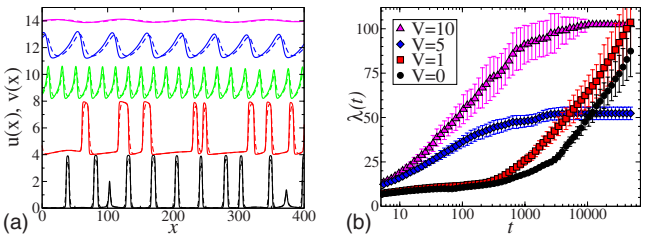

FIG. 3. (Color online) (a) Density u (solid line) and signal concentration v (dashed line) profiles at $t=3500$ for (bottom to top) $V=0$, 1, 2, 5, and 10 (profiles are offset vertically). (b) Temporal evolution of the lateral pattern wavelength $\lambda(t)$ for $V=0$ (black circles), $V=1$ (red squares), $V=5$ (blue diamonds), and $V=10$ (magenta triangles). Error bars represent the standard deviation calculated from 150 different random initial conditions.

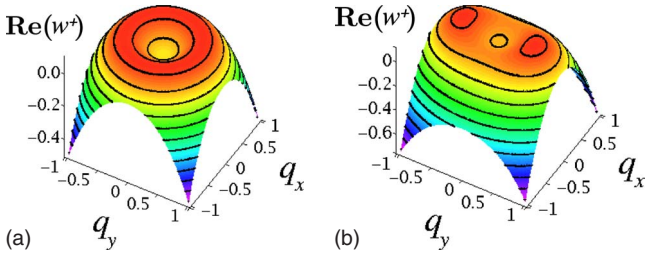

FIG. 4. (Color online) Real part of the dispersion relation $\mathrm{Re}(\omega^+)$ given by Eq. (10) as a function of q_x and q_y for a 2D system with (a) $V=0$ and (b) $V=2$.

for strong enough advection values (larger than V_t) coarsening is interrupted and the wavelength of the pattern becomes constant with a final value which is proportional to V as predicted by the linear analysis [see Fig. 1(b)]. Thus, the nonlinear effects (such as coarsening) are avoided for large values of V and the system remains in the linear regime. Similar results are obtained for the standard KS model, $\chi(u)=\chi_0 u$, with the difference that for slow advection the numerical simulations do not reach a stationary state, indicating an aggregation singularity with unlimited growth of the density in some points.

V. PATTERN FORMATION IN TWO DIMENSIONS

The effect of the advection term in the real part of the dispersion relation given by Eq. (10) for a 2D system is shown in Fig. 4. Without loss of generality we assume that the advection is along the x axis. Thus, we can write $\mathbf{V}=(V,0)$ and we plot $\mathrm{Re}(\omega^+)$ as a function of q_x and q_y for different values of V. When $V=0$ the system is isotropic and all the wave vectors within a distance q^l from the origin maximize $\mathrm{Re}(\omega^+)$ [Fig. 4(a)]. When V is nonzero, the maximum is oriented along the y axis but the absolute value is not affected by the value of V [Fig. 4(b)]. The effect of the advection on the wavelength and orientation of the pattern can be analyzed in the small q limit using Eq. (13). It can be shown that the dominant mode is always oriented along the y axis and its value is $q_y^l=[\nu/(2\mathcal{K}_y)]^{1/2}$, where $\mathcal{K}_y=\chi(1)[(1-D)+\chi(1)]$ and ν is the same as defined for the 1D case (see the Appendix). Thus, in contrast to the one-dimensional system, the observed dominant wavelength of the pattern in the linear regime is independent of the advection velocity V, although the features of the pattern are altered by the symmetry breaking induced by the advection. For the phase velocity, using the expansion of $\mathrm{Im}(\omega^+)$ for small q and Eq. (12) we have $\mathbf{V}^l\cdot\mathbf{q}^l/q^l=\chi(1)q^l(\mathbf{V}\cdot\mathbf{q}^l)=0$ because $\mathbf{V}=(V,0)$ and $\mathbf{q}^l=(0,q_y^l)$. Therefore, the dominant mode in the pattern is not moving since it is oriented in the y axis that is perpendicular to the advection velocity. However, for modes in the x axis, q_x, the phase velocity in this direction is $V_x^l=\chi(1)q_x^2V$, which is proportional to the advection velocity and increases with the wave number.

Two-dimensional numerical simulations were performed using a cubic interpolation semi-Lagrangian scheme [26] for the advection. For the spatial discretization of the particle density we used the method proposed recently by Grima and

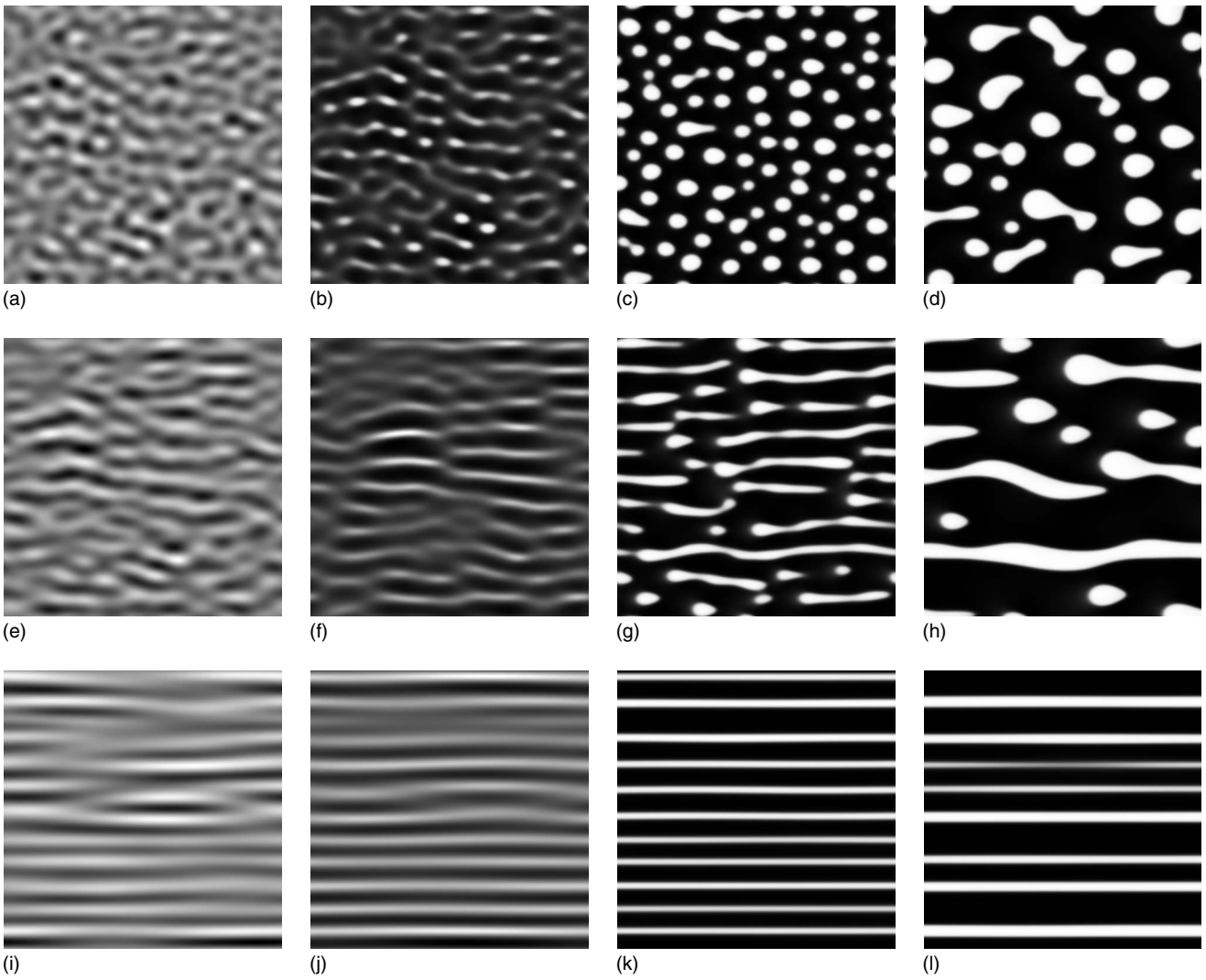

FIG. 5. Temporal evolution of u for different values of the advection velocity: $V=1$ (first row), 2 (second row), and 10 (third row); and different times: $t=35$ (first column), 70 (second column), 200 (third column), and 870 (fourth column). The x axis is horizontally oriented and the system size is 128×128. See also supplementary movies [28].

Newman [27] that allows for an accurate analysis of the evolution of the system without the dissipative effects of other schemes. In the absence of advection a slow coarsening process occurs in which, after long times, the organisms accumulate into a single aggregate [19]. When advection takes place the resulting pattern is not isotropic and the dominant wave vector is oriented along the y axis. The temporal evolution of u for different values of the advection velocity is shown in Fig. 5. As in the 1D case, the evolution of the chemical field is very similar to the density field (see supplementary movies [28]). As predicted above, the pattern does not propagate in the y direction and the coarsening process along the y axis is not affected by the advection (see supplementary movies [28]). Thus, in this direction the pattern features remain the same when the advection velocity is increased. A different scenario is found in the x direction where the pattern moves with a velocity which increases with V. The simulations also show that smaller aggregates move faster than larger ones, consistent with the dependence of the phase velocity on the wave number in the linear analysis. As in the 1D case, the characteristic wavelength of the pattern in the x direction increases with V. For slow advection there is a clear coarsening which leads to smaller propagation velocity of the aggregate as predicted above. For finite system sizes and large values of the advection velocity, the wavelength of the dominant linear instability in the x direction becomes larger than the system size and the resulting pattern is homogeneous in the x direction, observing a static pattern in this direction (see Fig. 5 for $V=10$).

VI. CONCLUSIONS

In this work we have studied theoretically how an advected uniform flow influences the aggregation dynamics in Keller-Segel-type models. We found that, in the presence of a differential flow, an advective instability produces a pattern moving in the direction of the flow. Interestingly, although the organisms are not directly advected, the advection of the

chemotactic signal induces a movement of the particle density as the organisms try to follow regions of high chemical concentrations. When the organisms mobility due to chemotaxis is weak in comparison to the advective flow (which is typically much faster), the balance between the chemotactic flux of the organism density and the advective transport of the chemical field breaks down, and it is then restored by a change in the characteristic of the spatial patterns that become strongly anisotropic with elongated stripelike structures aligned to the direction of the flow. Furthermore, as shown above, for flows larger than a certain threshold the organism cannot follow the chemotaxis signal reducing their velocity and eventually preventing the formation of large aggregates. Thus, the presence of a linear advection term inhibits the formation of large gradients and diminishes the nonlinear effects. This stabilizing effect may completely stop the chemotactic aggregation and the coarsening process in the direction of the flow. Although a simple unidirectional flow cannot suppress the coarsening in the perpendicular direction, preliminary results with more general nonuniform time-dependent velocity fields in two dimensions show that aggregation may be halted preventing the appearance of singularities associated with the KS models. This is similar to the arrested coarsening process observed in binary mixtures [29,30].

The theoretical results on the distribution of chemotactic cell populations under the influence of a differential flow are relevant for various natural and artificial systems including biofilms and could also be studied experimentally in the context of *Dictyostelium* aggregation. This work may also provide a starting point for the study of more general biological pattern formation phenomena in advected environments.

ACKNOWLEDGMENTS

This work was supported by a Science Foundation Ireland RFP research grant and a Centre for Science Engineering and Technology grant for SBI. Computational facilities were provided by ICHEC.

APPENDIX: LINEAR PATTERN ORIENTATION

The experimentally observed pattern is mainly oriented along the direction which yields the maximum value of the real part of the dispersion relation, and its wavelength is associated with the wave vector $\mathbf{q}^l=(q_x^l,q_y^l)$. This vector verifies

$$\left[\frac{\partial\,\mathrm{Re}(\omega^+)}{\partial q_x}\right]_{\mathbf{q}^l}=\left[\frac{\partial\,\mathrm{Re}(\omega^+)}{\partial q_y}\right]_{\mathbf{q}^l}=0, \tag{A1}$$

which have the following real independent solutions:

$$\mathbf{q_0}=(0,0),\quad \mathbf{q_1}=\left(\sqrt{\frac{\nu}{2\mathcal{K}}},0\right),\quad \mathbf{q_2}=\left(0,\sqrt{\frac{\nu}{2\mathcal{K}_y}}\right), \tag{A2}$$

where ν, $\mathcal{K}$, and $\mathcal{K}_y$ are defined as in the main text and assumed to be positive. In order to decide which of the remaining solutions provide the absolute maximum of $\mathrm{Re}(\omega^+)$, we finally substitute the wave vectors given by Eq. (A2) into Eq. (13); we obtain simply

$$[\mathrm{Re}(\omega^+)]_{\mathbf{q_0}}=0,\quad [\mathrm{Re}(\omega^+)]_{\mathbf{q_1}}=\frac{\nu^2}{4\mathcal{K}},\quad [\mathrm{Re}(\omega^+)]_{\mathbf{q_2}}=\frac{\nu^2}{4\mathcal{K}_y}, \tag{A3}$$

from where, since $\mathcal{K}>\mathcal{K}_y$ for $V\neq 0$, we conclude that $\mathbf{q}^l=\mathbf{q_2}$.

[1] A. Anderson and M. Chaplain, Bull. Math. Biol. **60**, 857 (1998).
[2] H. C. Berg, Phys. Today **53**(1), 24 (2000).
[3] N. Blackburn, T. Fenchel, and J. Mitchell, Science **282**, 2254 (1998).
[4] E. Budrene and H. Berg, Nature (London) **349**, 630 (1991).
[5] E. F. Keller and L. A. Segel, J. Theor. Biol. **26**, 399 (1970).
[6] R. M. Donlan, Emerg. Infect. Dis. **8**, 881 (2002).
[7] T. R. Neu and J. R. Lawrence, FEMS Microbiol. Ecol. **24**, 11 (1997).
[8] P. Stoodley, I. Dodds, J. D. Boyle, and H. M. Lappin-Scott, J. Appl. Microbiol. **85**, 19 (1999).
[9] T. J. Battin, L. A. Kaplan, J. D. Newbold, X. Cheng, and C. Hansen, Appl. Environ. Microbiol. **69**, 5443 (2003).
[10] S. Takayama, J. C. McDonald, E. Ostuni, M. N. Liang, P. J. A. Kenis, R. F. Ismagilov, and G. M. Whitesides, Proc. Natl. Acad. Sci. U.S.A. **96**, 5545 (1999).
[11] D. G. Davies, M. R. Parsek, J. P. Pearson, B. H. Iglewski, J. W. Costerton, and E. P. Greenberg, Science **280**, 295 (1998).
[12] E. Décavé, D. Garrivier, Y. Bréchet, B. Fourcade, and F. Bruckert, Biophys. J. **82**, 2383 (2002).
[13] E. Décavé, D. Rieu, J. Dalous, S. Fache, Y. Bréchet, B. Fourcade, M. Satre, and F. Bruckert, J. Cell Sci. **116**, 4331 (2003).
[14] T. Hillen and K. Painter, J. Math. Biol. **58**, 183 (2009).
[15] A. B. Rovinsky and M. Menzinger, Phys. Rev. Lett. **69**, 1193 (1992).
[16] A. B. Rovinsky and M. Menzinger, Phys. Rev. Lett. **72**, 2017 (1994).
[17] P. R. Fisher, R. Merkl, and G. Gerish, J. Cell Biol. **108**, 973 (1989).
[18] V. Nanjundiah, J. Theor. Biol. **42**, 63 (1973).
[19] T. Hillen and K. Painter, Adv. Appl. Math. **26**, 280 (2001).
[20] D. Horstmann, Jahresber. Dtsch. Math.-Ver. **105**, 103 (2003).
[21] D. Horstmann, Jahresber. Dtsch. Math.-Ver. **106**, 51 (2004).
[22] P. Chavanis, Eur. Phys. J. B **62**, 179 (2008).
[23] P. Chavanis, Eur. Phys. J. B **52**, 433 (2006).
[24] A. Mostowski and M. Stark, *Introduction to Higher Algebra* (Pergamon Press, Oxford, 1964).
[25] R. M. M. Mattheij, S. W. Rienstra, and J. H. M. T. T. Boonkkamp, *Partial Differential Equations: Modeling, Analysis, Computation* (Society for Industrial and Applied Math-

ematics, Philadelphia, PA, 2005).
[26] D. R. Durran, *Numerical Methods for Wave Equations in Geophysical and Fluid Dynamics* (Springer-Verlag, New York, 1999).
[27] R. Grima and T. J. Newman, Phys. Rev. E **70**, 036703 (2004).
[28] See EPAPS Document No. E-PLEEE8-80-160911 for the system evolution movies. For more information on EPAPS, see http://www.aip.org/pubservs/epaps.html.
[29] S. Berti, G. Boffetta, M. Cencini, and A. Vulpiani, Phys. Rev. Lett. **95**, 224501 (2005).
[30] L. Ó Náraigh and J.-L. Thiffeault, Phys. Rev. E **75**, 016216 (2007).